Name: Gregor Siegert
Institute: German Aerospace Center, Institute of Communications and Navigation
Address: Kalkhorstweg 53, 17235 Neustrelitz, Germany
Phone: +49 3981 480206
E-Mail address: gregor.siegert@dlr.de

MULTI-RADAR MULTI-TARGET TRACKING IN THE CONTEXT OF COOPERATIVE MARITIME TRAFFIC SITUATION ASSESSMENT

TABLE OF CONTENTS

INTRODUCTION

The challenges faced by the maritime world are manifold: the ever increasing global trade constantly calls for ships greater in size and numbers, which still need to traverse the international waterways and harbors in a secure and efficient manner. In addition, it is a stringent necessity to detect abnormal vessel behavior, to prevent harm to humans and nature. Migrant vessels or illegal fishing activities are merely two prominent examples. Apart from that, the trend towards autonomous navigation is clearly entering the maritime world calling for advanced solutions as enabling technologies. In future, a fleet of autonomous vessels will certainly involve more sensors, more data and more interaction among the traffic participants to grant efficient and secure shipping. Our today's concept of rather self-contained, individually navigating vessels will most probably be moved towards a scenario in which the navigation of all participants must be orchestrated among each other in a decentralized manner. From our perspective two conclusions can be drawn from these considerations: firstly, maritime situation awareness is crucial to all of these applications and secondly, the described challenges call for a refined and more reliable situation picture. To achieve the latter, we propose to conceive each vessel or shore-based monitoring station as potential node in a spatially distributed sensor network, in which information of individual sources is made available for further processing. A variety of benefits can be identified from such a cooperative approach for traffic situation assessment: spatially distributed sensors with different aspect angles provide diversity that can be exploited to obtain a higher accuracy of the pictured scene. Additionally, by introducing redundancy to the system, its reliability and robustness are improved. Failing sensors of single vessels can be compensated to a certain degree and even more important, individuals that do not act cooperatively, e.g., falsifying information intentionally, can be better identified by the community and excluded from the network. Conceptually, each traffic participant, may it be vessel or control station, can be understood as a spatially distributed sensor node within such a decentralized network. Each of these nodes collects, processes and shares information with potentially all of its peers. For instance, a single vessel would not solely rely on its own radar, but may also fuse it with the overlapping radar responses of adjacent ships for computing a refined situation picture of its surrounding. If all other vessels proceed similarly within their geographical area of interest and share this data, the merged situation picture of the current scene will be much closer to the overall truth than any of the single samples. The primary sensor for situation assessment and collision avoidance in the maritime domain is still the radar, which is installed at every shore-based control station and nearly every vessel. In 2004, the Automatic Identification System (AIS) was additionally introduced as supplemental service, which allows vessels and base stations to broadcast their dynamic state within a range of up to 40 NM.

In this study, we will demonstrate how to benefit from the cooperative approach for traffic situation assessment in the maritime domain. The assessed situation picture should at least contain the position of any detected object and its current dynamic state. Therefore, we will focus on the methodology for multi-target tracking based on multi-sensor fusion, while the latter describes the fusion of multiple distributed marine radars together with AIS data.

In the literature various approaches have been published to augment maritime surveillance or collision avoidance systems, mostly based on radar target fusion with additional sensors like laser in Perera et al. (2015) or multiple stationary radar systems for exploiting aspect angle diversity as in Braca et al. (2012). The matter of AIS and radar fusion was mainly addressed for anomaly detection, e.g., based on multi hypothesis tests in Guerriero et al. (2008) or by exploiting historical traffic route knowledge together with Synthetic Aperture Radar (SAR)/AIS fusion in Mazzarella and Vespe (2015). In Kazimierski and Stateczny (2015) an overview was given for different AIS/radar fusion techniques incorporating online covariance estimation. In (Siegert et al., 2016; Siegert et al., 2017), implementations of probabilistic data association filters were applied and tested for on-board maritime traffic situation assessment considering single and multiple targets in a clutter environment, respectively.

The remainder of this document is is organized as follows. A comprehensive overview to the proposed methodology for multi radar fusion and multi-target tracking is presented in Section 1. This framework will be evaluated in Section 2 based on measurement data. A conclusion and outlook is given in Section 3.

1. METHODOLOGY

Different strategies can be considered for fusing sensor data from multiple distributed radars. Drummond and Blackman (1989) distinguish between four different types of sensor network configurations. Within a configuration of type I each sensor is tracking independently without any sensor-to-sensor interaction, whereas the computed tracks of individual sensors are fused in a type II configuration. In this work, we focus on a type III configuration as it appears to be most promising in terms of uncertainty reduction and tractable complexity. Following this architecture the pre-processed measurements from individual but distributed sensors are associated to each other and fused prior to any centralized measurement-to-track association and actual target tracking. In contrast to that, all raw sensor measurements would be used for centralized measurement-to-track association and target tracking in a type IV configuration. In Figure 1 the generic framework for traffic situation assessment based on multi-radar and AIS fusion is presented, which will be explained in more detail in the following.

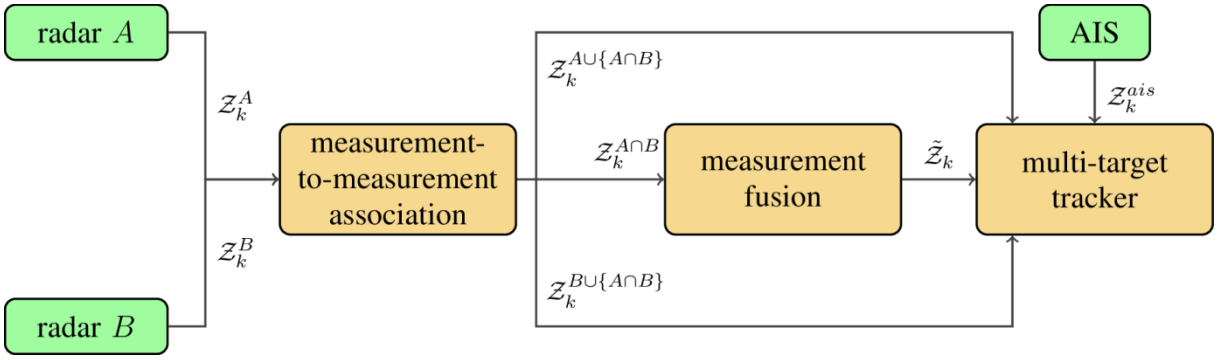

Figure 1: Block diagram of the proposed system architecture. At time k each of the radars A and B provide a set of measurements $\mathcal{Z}_k^A$ and $\mathcal{Z}_k^B$. The measurements that can be associated to each other constitute the subset $\mathcal{Z}_k^{A\cap B}$. The associated pairs within this set are fused yielding $\tilde{\mathcal{Z}}_k$, which is used as input to the multi-target tracker. The remaining measurements from radar A and B are captured in $\mathcal{Z}_k^{A\cup\{A\cap B\}}$ and $\mathcal{Z}_k^{B\cup\{A\cap B\}}$, respectively, and are directly used as measurement input to the tracker. In case the AIS provides a set of new measurements at time k, it is also used to update the multi-target state estimate.

1.1. RADAR MEASUREMENT FUSION

In a type III configuration the measurements of distributed sensor sources are fused prior to the actual tracking. The outcome of this process is treated as a single measurement input to the central tracker. The uncertainty of this abstract sensor, however, is time-variant and depends on the aspect angles between the radars. The framework to fuse different radar

measurements is presented in the following. Consider a single vessel located within the overlapping area of both marine radars as is depicted in Figure 2.

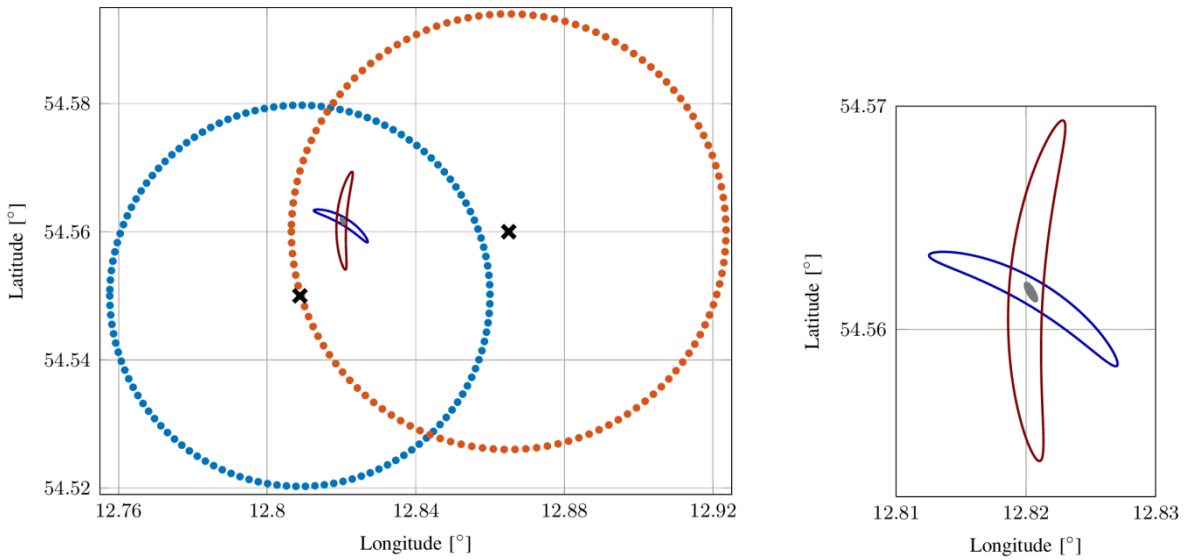

(a) Two radar systems at different locations (black crosses), with different ranges (blue and red dotted circles). A target (grey blob) is located within the overlapping area and detected by both radars.

(b) The measurement uncertainty is projected as banana shape in Car-tesian coordinates (dark blue, dark red).

Figure 2: Sample setup to visualize sensor fusion for two radars at capturing the same target from different aspect angles.

Assuming radar s has detected the target, we obtain a sensor measurement $\mathbf{z}_s^k$ that represents the true target position with a certain probability following the distribution of

$$p(\mathbf{z}_k^s) \sim \mathcal{N}(\boldsymbol{\mu} = \mathbf{z}_k^s, \boldsymbol{\Sigma} = \mathbf{R}_k^s) \tag{1}$$

at time k. In other words, the target measurement is described via the mean and its corresponding covariance. In radar technology the measurement domain is equivalent to the polar coordinate frame, which is referenced to the radar's position. This implies that the measurement vector $\mathbf{z}_s^k$ becomes $[r_s, \theta_s]^T$, capturing the range r and bearing θ of the target at time k w.r.t. radar s. The uncertainty of the detection is typically accounted in

$$\mathbf{R}_k^s = \begin{bmatrix} \sigma_{s,r}^2 & 0 \\ 0 & \sigma_{s,\theta}^2 \end{bmatrix}, \tag{2}$$

with $\sigma_{s,r}$ and $\sigma_{s,\theta}$ being the expected standard deviation in range and bearing. In order to fuse two measurements, we will simply collapse both overlapping distributions to a single Gaussian, with a merged covariance and a shifted mean. The basic prerequisite to fuse both distributions is to have them represented in the same reference frame. Hence, we need to transform them from their local measurement domain to a global coordinate system. At first, we transform the polar to local Cartesian coordinates following

$$\begin{bmatrix} x_k^s \\ y_k^s \end{bmatrix} = \begin{bmatrix} r_k^s \sin(\theta_k^s) \\ r_k^s \cos(\theta_k^s) \end{bmatrix}, \tag{3}$$

with θ_k^s, i.e., the bearing, being defined as the angle which is spanned between the axis pointing North and the vector pointing to the detected target in clockwise direction. In fact, the vector $\left[x_k^s, y_k^s\right]^T$ is already defined in the local East-North-Up (ENU) frame with the radar in its origin. In a second step, these coordinates are translated from the local ENU to the global Earth-Centered, Earth-Fixed (ECEF) reference frame. Once we have obtained both measurements in the same coordinate system we can transform them back to a Cartesian plane by choosing the identical reference point for both of them. However, this only applies to the target measurement $\mathbf{z}_k^s$ in range and bearing. The covariance of the measurement $\mathbf{R}_k^s$, i.e., the sensor uncertainty, remains aligned with the radial axis of the corresponding radar. In the polar domain a Gaussian distribution is assumed to be centered at $\mathbf{z}_k^s$ with a covariance in range and bearing, following Equation 1. If this is mapped to the Cartesian plane the ellipsoidal contour of the normal distribution is projected onto a banana shaped uncertainty region, which is depicted in Figure 2(***b***. To avoid the non-trivial analytical expression in Cartesian coordinates of the original Gaussian distribution in the polar measurement domain, we will approximate the whole uncertainty area again with a Gaussian, which is defined as

$$pdf \sim \mathcal{N}\left(\boldsymbol{\mu} = \begin{bmatrix} x_k^s \\ y_k^s \end{bmatrix}, \boldsymbol{\Sigma} = \widetilde{\mathbf{C}}_k^s\right), \text{ with } \widetilde{\mathbf{C}}_k^s = \begin{bmatrix} \sigma_{\tilde{x}}^2 & 0 \\ 0 & \sigma_{\tilde{y}}^2 \end{bmatrix}. \tag{4}$$

The standard deviations in $\tilde{x}$ and $\tilde{y}$ are approximated by the assumptions $\sigma_{\tilde{y}} = \sigma_r$ and $\sigma_{\tilde{x}} = r_k \sigma_\theta$. The former holds true, since radial and $\tilde{y}$-axis are equivalent; the latter approximates the uncertainty in the tangential direction, i.e., $\tilde{x}$-axis, with the arc length, which scales with the uncertainty in bearing and the range of the target. Figure 3(*a* shows the outcome of this simplification by plotting the contour lines of the 3σ threshold on top of the originally bended uncertainty regions. The approximated Gaussians, however, representing the uncertainty of the measurement in Cartesian coordinates are still aligned with the radial and tangential direction of the radar. This needs to be compensated by rotating the covariances back into the same reference frame yielding a generalized, non-diagonal covariance

$$\mathbf{C}_k^s = \begin{bmatrix} \sigma_x^2 & \rho\sigma_x\sigma_y \\ \rho\sigma_y\sigma_x & \sigma_y^2 \end{bmatrix}, \tag{5}$$

aligned with the x- and y-axes of the reference ENU frame.

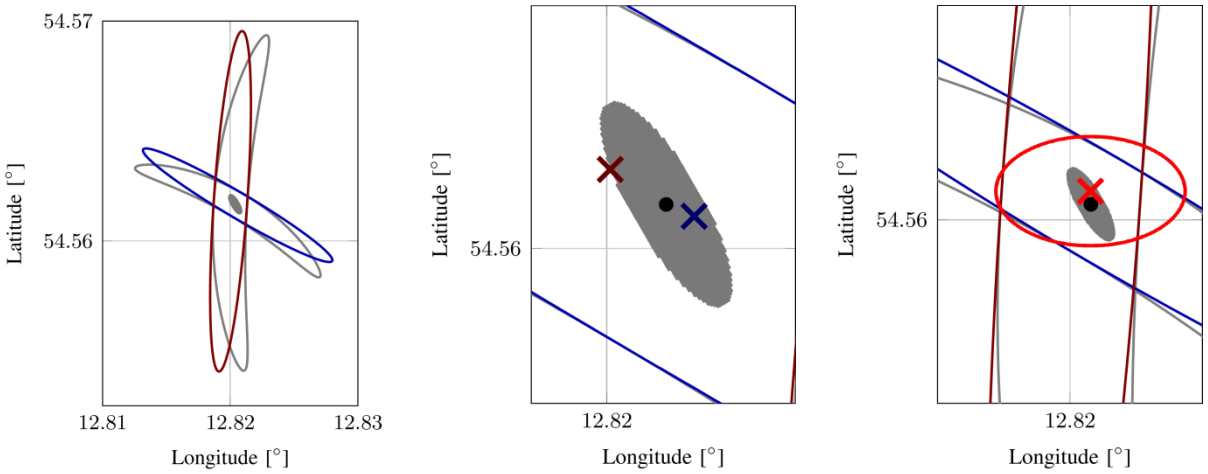

(a) The radar uncertainty regions (banana shaped projections in grey) are approximated by Gaussians (red and blue).

(b) The detected target positions (mean of uncertainty region) as red and blue crosses for each radar.

(c) Fused target candidate with a shifted mean and reduced uncertainty.

Figure 3: Radar fusion process in Cartesian domain for a single target.

Any affine transformation $\mathbf{F}$ on the state vector $\mathbf{x}_k$ becomes

$$\mathbf{C}_k^s = \mathbf{F}\mathbf{C}_k^s\mathbf{F}^T \tag{6}$$

in case of transforming the covariance to the same domain. Thus, to align the covariance matrix with the x- and y-axis of the ENU reference frame we need to rotate the matrix $\widetilde{\mathbf{C}}_k^s$ by the bearing angle θ^s according to

$$\mathbf{C}_k^s = \mathbf{R}(\theta^s)\widetilde{\mathbf{C}_k^s}\mathbf{R}(\theta^s)^T, \tag{7}$$

with $\mathbf{R}(\cdot)$ being defined on counter-clockwise rotations. Now, very similar to the correction step of the Kalman Filter in Kalman (1960) we can collapse both Gaussians into one. In general, considering two distributions the covariance and the shifted mean of the fused Gaussian are obtained from

$$\mathbf{C}_k = \mathbf{C}_k^1 - \mathbf{C}_k^1\left[\mathbf{C}_k^1 + \mathbf{C}_k^2\right]^{-1}\mathbf{C}_k^{1\,T} \tag{8}$$

and

$$\boldsymbol{\mu}_k = \boldsymbol{\mu}_k^1 + \mathbf{C}_k^1\left[\mathbf{C}_k^1 + \mathbf{C}_k^2\right]^{-1}\left[\boldsymbol{\mu}_k^2 - \boldsymbol{\mu}_k^1\right]. \tag{9}$$

The entire process is visualized in Figure 4(*a* and Figure *4*(*b* for the same generic scenario that was shown in Figure 2 and Figure 3. In a last step, the fused covariance $\mathbf{C}_k$ needs to be rotated back into the ENU reference frame, as it will be misaligned with its axes.

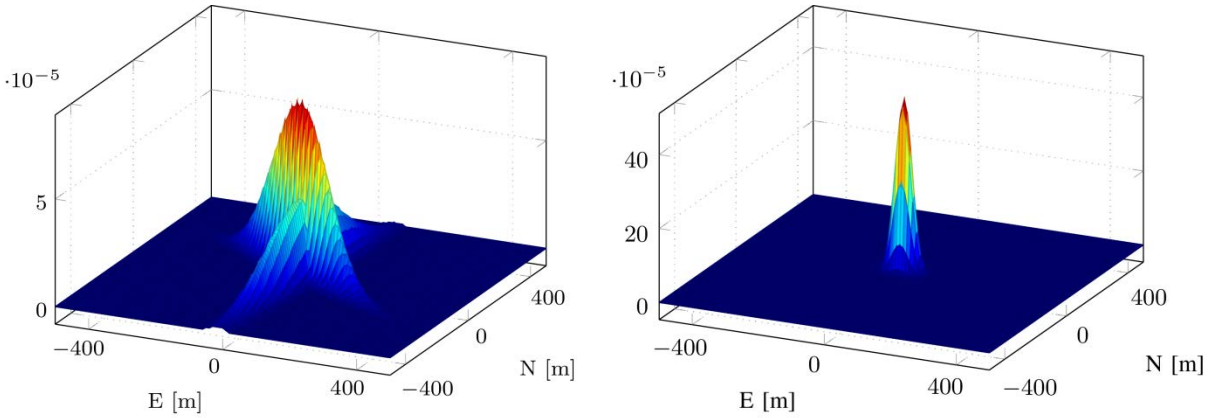

(a) Both Gaussians overlap in ENU frame. *(b) Merged Gaussian in ENU frame.*

Figure 4: Sensor fusion by merging two radar target detections. Each target is described via its mean and its covariance, which is in fact the corresponding sensor uncertainty.

The new orientation $\tilde{\theta}$ of the merged covariance can be obtained from eigenvalue decomposition. If we take the eigenvector $\mathbf{v}$ that corresponds to the largest eigenvalue of $\mathbf{C}_k$, we obtain $\tilde{\theta}$ from

$$\tilde{\theta} = \arctan\left(\frac{v_y}{v_x}\right). \tag{10}$$

This time, the angle $\tilde{\theta}$ is defined in counter-clockwise direction, spanning from the x-axis to the eigenvector $\mathbf{v}$ in the ENU frame. With this in mind, we need to plug in $-\tilde{\theta}$ to Equation 7 for clockwise rotation.

1.2. RADAR MEASUREMENT-TO-MEASUREMENT ASSOCIATION

Prior to fusing radar target measurements we need to associate these measurements obtained from different sensor sources. This becomes evident, by considering a single radar scan, which will typically contain not a single but a number of detections. In this work, we propose a two-step procedure to find the correct measurement-to-measurement associations:

1) At first, N_A measurements from radar A need to be paired with N_B measurements from radar B. A Global Nearest Neighbor (GNN) rule is applied, which yields bijective associations based on the inter measurement distance. The Munkres algorithm is an efficient implementation to find the correct pairing (Munkres, 1957).

2) Secondly, each associated pair of measurements needs to pass an additional hypothesis test prior to be fused. We are testing for hypotheses:

   H_0 : both measurements origin from the same target

H_1: measurements origin from different targets/clutter

For this purpose we exploit the approximate model of the measured radar target candidate's position via its mean and its corresponding covariance, i.e., the sensor uncertainty. This allows the computation of the Bhattacharyya similarity measure from (Bhattacharyya, 1946) between both distributions, from radar A and radar B. Only if the Bhattacharyya coefficient exceeds a certain threshold h_B, H_0 is accepted and both measurements are fused according to the scheme described in 1.1.

In principle, the Bhattacharyya measure computes the distance D_B between two distributions, which is closely linked to the Bhattacharyya coefficient BC. The latter expresses the amount of overlap between both distributions. In case of two normal distributions p and q, these measures are defined as

$$D_B(p,q) = \frac{1}{8}\left(\boldsymbol{\mu}_p - \boldsymbol{\mu}_q\right)^T \boldsymbol{\Sigma}^{-1}\left(\boldsymbol{\mu}_p - \boldsymbol{\mu}_q\right) + \frac{1}{2}\ln\left(\frac{\det\boldsymbol{\Sigma}}{\sqrt{\det\boldsymbol{\Sigma}_p \det\boldsymbol{\Sigma}_q}}\right), \tag{11}$$

with $\boldsymbol{\Sigma} = \frac{\boldsymbol{\Sigma}_p + \boldsymbol{\Sigma}_q}{2}$ and $D_B(p,q) = -\ln\left(BC(p,q)\right)$.

1.3. MULTI-TARGET TRACKING IN AN IMM-JPDA FRAMEWORK

In general, the field of multi-target tracking (MTT) in presence of multiple and in general imperfect sensors has been widely explored, ranging from classical enumerative to non-enumerative schemes. Algorithms representing the former category, such as GNN and Joint Probabilistic Data Association (JPDA) filtering, integer programming or Multi Hypothesis Tracking (MHT) are well described in (Pulford, 2005; Bar-Shalom et al., 2009; Khaleghi et al., 2013). More recent work has also applied random finite set (RFS) theory to MTT yielding the Probability Hypothesis Density (PHD) or Cardinalized PHD (CPHD) filters (Mahler, 2015). The extension of these frameworks to the case of distributed target tracking has for instance led to the generic formulation of Distributed MHT (Coraluppi et al., 2015). For tracking vessels of various types, we assume to propagate the state vector $\mathbf{x}_{k-1}^t$ of the t^{th} target to the next time frame k through a non-linear motion model following the notation of

$$\mathbf{x}_{k|k-1}^t = f^i(\mathbf{x}_{k-1}^t, \boldsymbol{\epsilon}_k^q), \tag{12}$$

where $\boldsymbol{\epsilon}_k^q \sim \mathcal{N}\left(\mathbf{0}, \Sigma = \mathbf{Q}_k^i\right)$. To distinguish between different dynamic models in the upcoming sections, we introduce the superscript i to the non-linear function $f^i(\cdot)$. The predicted state estimate $\mathbf{x}_{k|k-1}^t$ will be corrected by evaluating the residual between the actual measurement $\mathbf{z}_k^s$ of sensor s associated to the t^{th} target and the predicted measurement for that sensor following the general formulation of

$$\hat{\mathbf{z}}_{k|k-1}^s = h^s(\mathbf{x}_{k|k-1}^t, \boldsymbol{\epsilon}_k^r), \tag{13}$$

with $\boldsymbol{\epsilon}_k^r \sim \mathcal{N}\left(\mathbf{0}, \Sigma = \mathbf{R}_k^s\right)$. In the remainder of this section, we will introduce the implemented multi-target tracker and define the utilized set of dynamic and measurement models.

Considering the inherent trade-off between complexity and tracking performance a variation of the JPDA filter was chosen, being combined with an Interacting Mulitple Model (IMM) filter to capture different target dynamics. Being first introduced in Fortmann et al. (1983), the JPDA filter is subject to several assumptions. Most importantly for our application, the finite set of targets to be tracked is assumed to be known, i.e., neither track initialization nor track pruning is covered by the standard formulation of JPDA. These restrictions, however, are tolerable in our specific case of fusing radar target candidates with vessels visible in AIS. In fact, the number of targets to be tracked as well as their initial states are known from AIS within the considered measurement scenario. The key feature of the JPDA is the computation of conditional probabilities of joint association events

$$A(k) = \bigcap_{j=1}^{M} A_{jt}(k), \tag{14}$$

with respect to the current time k, in which $A_{jt}(k)$ represents the event of the j^{th} measurement originating from target t, with $1 \leq j \leq M$ and $0 \leq t \leq N$. In this context, M refers to the number of measurements at time k, N to the number of known targets and t_j is the target index the j^{th} measurement is associated to. With $t = 0$ the specific case of a measurement originating from clutter is also being considered. This means, in contrast to a nearest neighbor (NN) association rule, the JPDA also accounts for situations in which a single measurement can be assigned with certain likelihoods to multiple targets at the same time. Details can be found in (Fortmann et al., 1983; Bar-Shalom et al., 2009). It can easily be seen that the considerations of all joint events results in a combinatoric growth in complexity for more measurements and more targets. To narrow down the initial set of feasible association events a validation matrix $\mathbf{B}$ is usually computed first, which is a binary matrix of dimensionality $M \times (N+1)$ representing all possible associations between

measurements and targets. Whether the single matrix element b_{mt} is set to either 0 or 1 depends on classical validation gating, i.e., the condition of

$$[\mathbf{z}_j(k) - \hat{\mathbf{z}}_{t_j}(k \mid k-1)]^T \mathbf{S}_{t_j}^{-1}(k)[\mathbf{z}_j(k) - \hat{\mathbf{z}}_{t_j}(k \mid k-1)] < \gamma. \tag{15}$$

needs to be fulfilled for b_{mt} to become 1. Volume V of this gate depends on the innovation covariance $\mathbf{S}_{t_j}^{-1}(k)$. Despite this pre-selection of possible association events, various additional flavors of the JPDA filter were introduced aiming at the reduction of combinatoric complexity (see Pulford (2005) for a comprehensive comparison).

In this work, we use an extension to classical JPDA filtering known as IMM-JPDA filter. The IMM was introduced by Blom and Bar-Shalom (1988) to adapt to quickly changing target dynamics by considering a finite set of kinematic models that run in parallel. In contrast to hard switching schemes, the IMM weighs the different target state estimates based on the likelihood of each model to explain the current measurement data. The mode transition is thereby governed by an underlying Markov chain. In our case, we consider a set of two dynamic models to capture either straight path or turning maneuver based motion. For the former a Constant Velocity (CV) model was designed, whereas the Constant Turn Rate Velocity (CTRV) model is supposed to fit best to the latter. The corresponding target state vectors are defined as

$$\mathbf{x}_k^{\mathrm{CV}} = \left[p_{e,k},\, p_{n,k}, \psi_k, v_k \right]^T, \qquad \mathbf{x}_k^{\mathrm{CTRV}} = \left[p_{e,k},\, p_{n,k}, \psi_k, v_k, \dot{\psi}_k \right]^T, \tag{16}$$

with $\{p_{e,k}, p_{n,k}\}$ being the 2D position coordinates in the local ENU frame, ψ_k the course over ground, v_k the speed over ground and $\dot{\psi}_k$ the turn rate at time k. The uncertainty within the models is expressed in

$$\mathbf{Q}_k^{\mathrm{CV}} = \begin{bmatrix} \sigma_\psi^2 & 0 \\ 0 & \sigma_v^2 \end{bmatrix}, \qquad \mathbf{Q}_k^{\mathrm{CTRV}} = \begin{bmatrix} \sigma_v^2 & 0 \\ 0 & \sigma_{\dot{\psi}}^2 \end{bmatrix}. \tag{17}$$

The detailed definitions of the process models $f^i(\cdot)$ for CV and CTRV can be found in Siegert et al. (2016). In many applications it can be beneficial to parameterize the different models in such a way that one acts more conservatively than the other. Applied to our case, the CV model is set to adapt to changes very slowly, i.e., the variances in $\mathbf{Q}_k^{\mathrm{CV}}$ are rather small. Vice versa, more uncertainty is allowed to the CTRV yielding a model more flexible to rapid changes. Additionally, careful attention needs to be paid to the augmentation of state vectors of different dimensions. In this paper we follow a strategy described in Glass et al. (2013) for unbiased mixing of different process models. In contrast to the common formulation of either IMM or JPDA, which both use Extended Kalman Filtering (EKF) to

adopt to non-linearities in the dynamic models, we deploy the Unscented Kalman Filter (UKF) instead (Julier and Uhlmann, 1997). It turns out that due to the sigma point sampling approach the UKF is more robust against non-linearities induced by the radar measurement update equation, whereas the approximation to a first-order Taylor series expansion within the EKF is not always sufficient (see Braca et al. (2012) for discussion). The combination of IMM and JPDA filtering schemes to a well-defined framework was initially proposed by Blom and Bar-Shalom (1988) and extended to the multi-sensor case in Tugnait (2003). In the end, a recursive step-by-step algorithm was derived fusing the asynchronous measurements from different sensors sequentially. The final state update equation for the t^{th} target tracked in mode $i \in \{\text{CV}, \text{CTRV}\}$ becomes

$$\mathbf{x}_{k|k}^{t,i} = \beta_{0t}^{i} \mathbf{x}_{k|k-1}^{t,i} + \sum_{j=1}^{M_{t,k}} \mathbf{x}_{k|k}^{t,i}(j) \beta_{jt}^{i}, \tag{18}$$

with $M_{t,k}$ being the number of validated measurements for target t and $\mathbf{x}_{k|k}^{t,i}(j)$ the UKF target estimate conditioned on the j^{th} measurement at time k. The weights β_{jt}^{i} are interpreted as association probabilities following the convention in Braca et al. (2012).

1.4. TARGET CANDIDATE EXTRACTION FROM RADAR IMAGES

Within the proposed multi-sensor architecture radar target measurements will be processed in two different ways: they will be either fused to obtain an abstract sensor measurement or directly used as measurement input to the target tracker. In either way, the corresponding target candidates need to be detected and extracted from the current radar frame first. The utilized approach to extract radar target information is based on image processing instead of directly working on the raw radar signal. This may introduce additional error sources originating from mapping the radar target data from signal to image domain, but also yields the advantage of applying the proposed technique to most commercial radar systems by simply interfacing to the video output. Additionally, it opens the opportunity for image based feature extraction to do extended target tracking in the future. To extract target candidates from the current radar image at time k, the following procedure is applied:

1) Masking the image to eliminate features of the user interface, e.g., colored heading lines, blob in center, radar information tables.
2) Conversion of the image from RGB to gray-scale (weighted average from color channels).
3) Blob detection with fixed range settings for convexity, circularity, inertia, size and intensity of expected targets.
4) Each detected target candidate per frame is expressed in range and bearing, relative to the position of the vessel carrying the radar.

The key aspect in this processing chain is certainly the scale-invariant blob detection to eventually detect target candidates. Various types of algorithms for blob detection can be found in the literature, e.g. for image based target detection and tracking in Isard and MacCormick (2001). For this work the implementation provided by the OpenCV framework was used[1]. Figure 5(*a) Original radar image.* to Figure 5(*c) Extracted target candidates (red circles).* show the different radar processing stages.

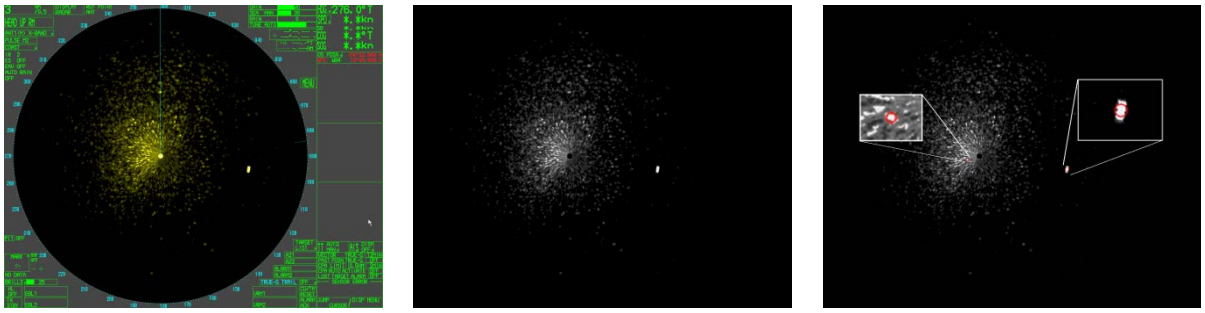

(a) Original radar image. *(b) Pre-processed image.* *(c) Extracted target candidates (red circles).*

Figure 5: Processing chain for one radar image at time k to extract the target candidates.

The set of extracted radar measurements is defined as $\mathcal{Z}_k^s = \{\mathbf{z}_k^1, \ldots, \mathbf{z}_k^M\}$, with the j^{th} measurement vector $\mathbf{z}_k^j = [z_k^r, z_k^b]^T$ comprising range and bearing of the target candidate. In case the target state $\mathbf{x}_{k|k-1}^i$ will be directly conditioned on the associated target measurements of a single radar, we need to incorporate a specific measurement model that transforms Cartesian state to polar measurement domain. Thus, the definition of $h^s(\mathbf{x}_{k|k-1}^i, \boldsymbol{\epsilon}_k^{r,s})$ from Equation 15 is given as

$$h^s(\mathbf{x}_{k|k-1}^i, \boldsymbol{\epsilon}_k^{r,s}) = \begin{bmatrix} \sqrt{(p_{e,k|k-1} - p_e^s)^2 + (p_{n,k|k-1} - p_n^s)^2} \\ \arctan\left(\dfrac{p_{n,k|k-1} - p_n^s}{p_{e,k|k-1} - p_e^s}\right) \end{bmatrix} + \boldsymbol{\epsilon}_k^{r,s}, \tag{19}$$

for $s \equiv radar$ and with $\{p_e^s, p_n^s\}$ being the 2D position coordinates of the radar in the reference ENU frame. The sensor uncertainty in range (σ_r) and bearing (σ_b) is modeled in

$$\mathbf{R}_k^{radar} = \begin{bmatrix} \sigma_r^2 & 0 \\ 0 & \sigma_b^2 \end{bmatrix}. \tag{20}$$

[1] OpenCV 3.1.0: https://github.com/Itseez/opencv.git

1.5. AIS TARGET DATA

A typical AIS data set contains numerous static and dynamic parameters that are distributed over different AIS message types and specified in the ITU-R recommendation (ITU-R, 2014). The set of dynamic parameters always comprises the vessel position in longitude and latitude, course over ground (COG) and speed over ground (SOG), but may also contain true heading and rate of turn (ROT) information. To integrate the AIS data to the tracking process we simply assign the AIS message to the t^{th} target via its unique Maritime Mobile Service Identity (MMSI). Instead of applying a probabilistic association scheme we set up a validation gate around the predicted target position in the measurement domain to reject outliers from AIS data. For state correction the AIS coordinates are converted from geodetic to the target's ENU frame that originates at the latest estimated target position in the global ECEF frame. This implies the AIS measurement vector $\mathbf{z}_k$ to be defined as $[z_k^e, z_k^n]^T$ and the corresponding measurement model from Equation 17 becomes

$$h^s(\mathbf{x}_{k|k-1}^t, \boldsymbol{\epsilon}_k^{r,s}) = \begin{bmatrix} p_{e,k|k-1} \\ p_{n,k|k-1} \end{bmatrix} + \boldsymbol{\epsilon}_k^{r,s}, \tag{21}$$

with $s \equiv AIS$ and the sensor noise in East and North coordinates being captured in

$$\mathbf{R}_k^{AIS} = \begin{bmatrix} \sigma_{p,e}^2 & 0 \\ 0 & \sigma_{p,n}^2 \end{bmatrix}. \tag{22}$$

Note that the update rate of AIS position reports is varying with the vessel's dynamics (ITU-R, 2014). This also implies that the AIS measurements are in principle asynchronous to measurements obtained from radar; we were grabbing images at a rate of approximately 0.5 Hz .

2. RESULTS

2.1. THE MULTI-RADAR EXPERIMENT IN THE BALTIC SEA

In June 2016, a dedicated measurement campaign was conducted in the Baltic Sea close to the island of Hiddensee, Germany, see Figure 6*Figure 1*.

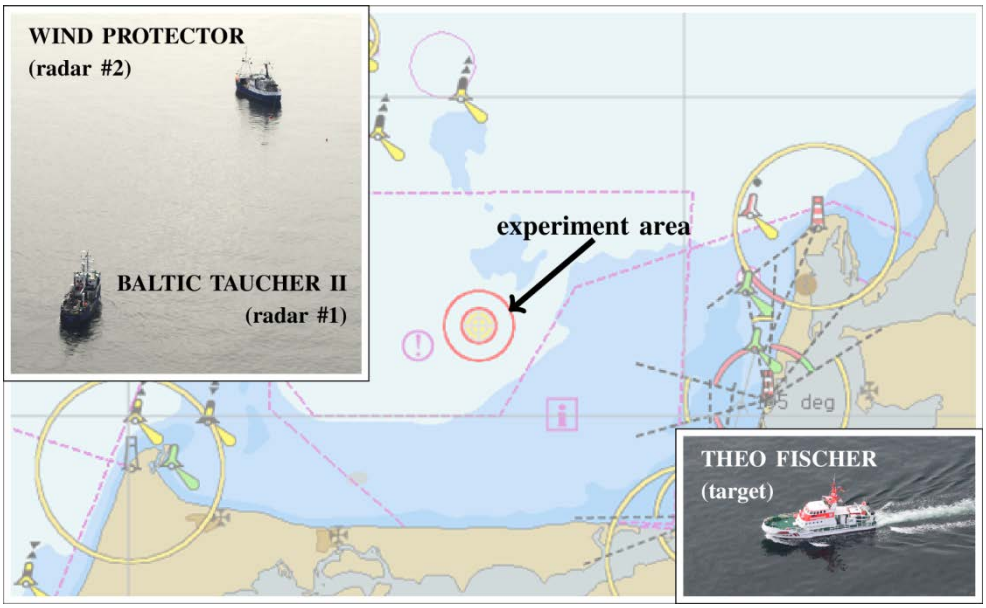

Figure 6: The measurement campaign was conducted in the Baltic Sea close to Hiddensee, Germany. Three vessels were involved, the BALTIC TAUCHER II as well as the WIND PROTECTOR, which acted both as sensor platforms carrying a radar each. The THEO FISCHER completed the scenario as mobile target, which was conducting sharp turns and straight path motion.

The campaign setup can be characterized as follows:

- Three vessels were involved in total
  - two chartered ships, BALTIC TAUCHER II (offshore supply vessel) and WIND PROTECTOR (small cargo vessel)
  - one external ship, THEO FISCHER (search-and-rescue vessel)
- Two radars were monitoring the test area, being installed on the anchored WIND PROTECTOR and the mobile BALTIC TAUCHER II
- THEO FISCHER performed dynamic maneuvers within the experiment area, acting as mobile target.

For evaluation purposes we selected a 30 min long snippet from the entire three day campaign. From this subset two multi-radar scenarios were generated:

- *Proof of principle by single target tracking* fusing both radars prior to data filtering in an IMM-PDA tracker. The aspect angles between both sensor vessels are ranging from 10° to 180°, while the target dynamics include straight paths and turn-maneuver motion.
- *Multi target tracking* according to the proposed algorithm from Figure 1: First, the measurements from both radars are associated and fused, if the Bhattacharyya test is passed. Second, a centralized IMM-JPDA tracker is conditioned on either the refined or individual radar measurements together with AIS data, if available. In total, four vessels will be tracked; two of them are also visible in AIS. The other two targets were fishing vessels, passing by, only visible in radar.

In Figure 7 we plotted the radar responses for both vessels monitoring the identical situation from different aspect angles.

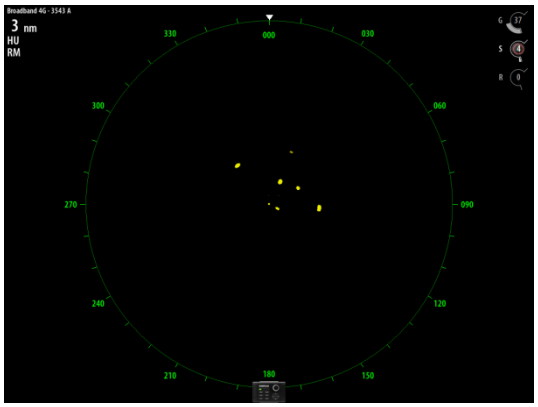

(a) Radar response at BALTIC TAUCHER II, with a maximum range of 3 NM.

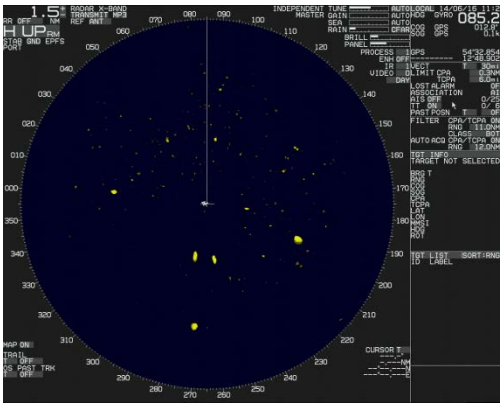

(b) Same situation observed by radar at WIND PROTECTOR with a maximum range of 1.5 NM.

Figure 7: Responses from both radars at arbitrary time instance k for the identical situation during measurement campaign.

All relevant IMM-JPDA parameter settings that were chosen during algorithm evaluation are listed in Table 1.

Table 1: Summary of parameter settings used for algorithm evaluation.

model uncertainty (**Q**)		sensor uncertainty (**R**)		JPDA settings	
CV	$\sigma_v = 0.01 \, m/s^2$, $\sigma_\psi = 0.01 \, ^\circ/s$	AIS	$\sigma_{p,e} = 5$ m, $\sigma_{p,n} = 5$ m	JPDA type	*parametric*
CTRV	$\sigma_v = 0.1 \, m/s^2$, $\sigma_{\dot{\psi}} = 0.1 \, ^\circ/s^2$	Radar #1	$\sigma_r = 25$ m, $\sigma_b = 1.0°$	spatial density λ	10^{-9}
		Radar #2	$\sigma_r = 40$ m, $\sigma_b = 0.75°$	$P_{d,radar\#1}$	0.9
				$P_{d,radar\#2}$	0.8

The threshold h_B introduced for hypothesis testing in Section 0 was set to 0.1 throughout this analysis. Only measurements from radar *A* and *B* that pass this test for similarity were fused.

Note that it was not possible to generate reference trajectories for all the vessels, i.e. the multi-target state reference is missing for both scenarios. This implies that we can test our algorithm only on a qualitative scale, focusing on track completeness and the ability to separate targets. A quantitative measure for performance evaluation cannot be given.

2.2. SCENARIO (1)

In this first experiment, we were interested in proving the basic assumptions of the proposed approach. Thus, we were focusing on a single target only analyzing the multi-radar performance in terms of uncertainty reduction with respect to the aspect angle between both radars. The expectation is clearly that the uncertainty of the fused radar measurements should be lowest for aspect angles close to $90°$. In Figure 8 we plotted all fused radar measurements, i.e., their fused mean values, into the reference ENU frame.

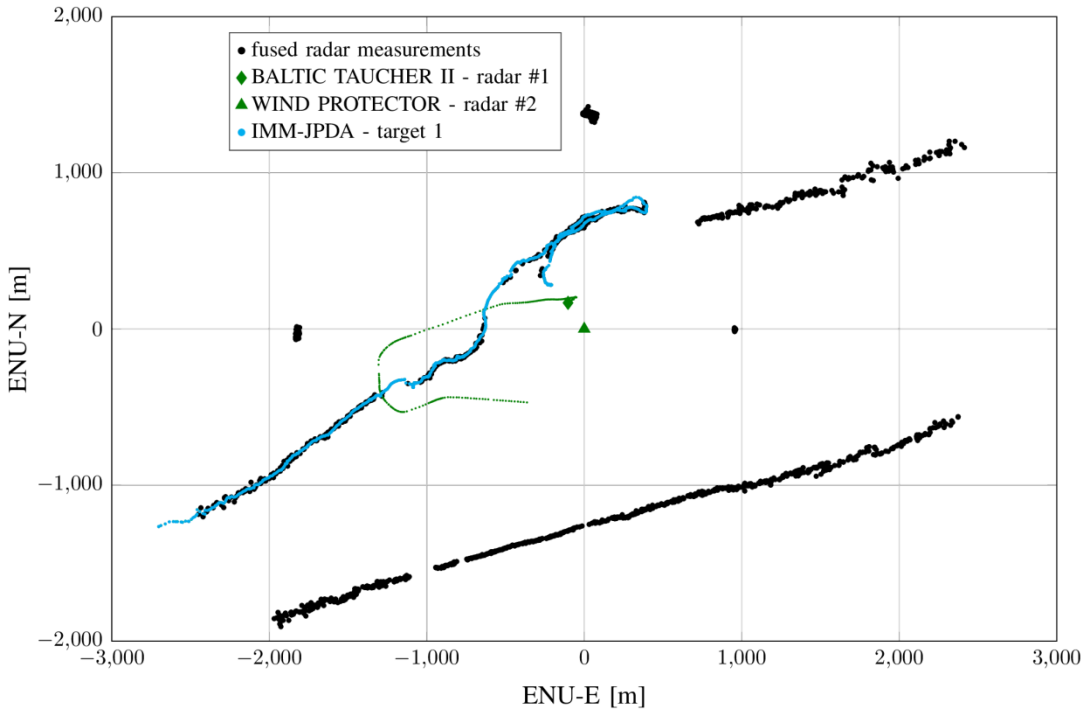

Figure 8: Resulting track for a single target obtained only by fusing both radars before updating the tracker (light blue dots). Both radar platforms are visualized as green diamond and triangle, respectively. The trace of the mobile radar platform is plotted as a dotted line. The fused radar measurements are represented by black dots. In this scenario multiple targets are visible in radar, whereas only one of them is being tracked.

On top of that the resulting track from the IMM-JPDA tracker is added. Note that in accordance to the architecture in Figure 1 this track is not solely conditioned on the fused, but also on individual radar measurements that did not pass the hypothesis test. This behavior becomes visible in the beginning of the track in the lower left corner of the ENU plot. At this stage, the target is only visible in radar #1 (installed on BALTIC TAUCHER II). Thus, the track is picked up already before both radar sensors can be fused. In fact, the covered range is extended in the situation picture assessed cooperatively compared to the standalone sensor approach. It is also worth mentioning that the radar measurements are dispersing at the edges of the target tracks. This is in fact a typical phenomenon as the uncertainty of the detection in tangential direction grows with bigger range.

Regarding the aspect angle dependency of the fused covariance we can conclude that the expectations are met. Figure 9 depicts not only the angle in (Figure 9(*a*) and the norm of the covariance (Figure 9(*b*) over time, but also the distribution of the norm of the covariance with respect to the aspect angle (Figure 9(*c*). For this single scenario, the distribution of the norm correlates with a convex function, with the minimum close to $90°$.

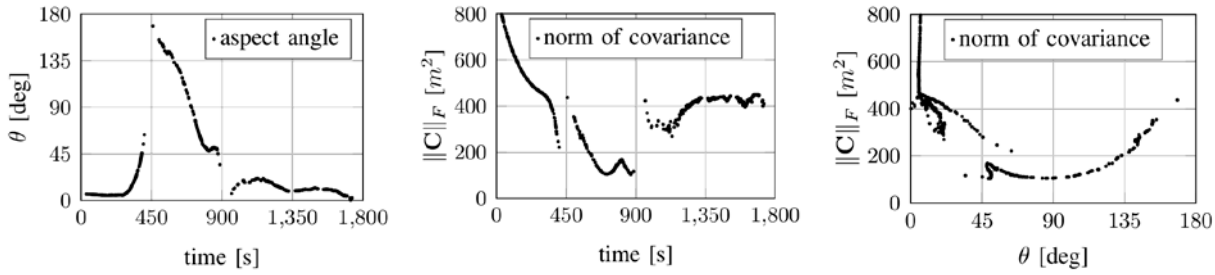

(a) Aspect angle between both radars over time.

(b) Norm of fused covariance over time.

(c) Norm of fused covariance against aspect angle.

Figure 9: Aspect angles between both radar platforms and norm of the fused covariance over time. With the aspect angle approaching 90 the uncertainty reduction of the fused measurement is maximized.

2.3. SCENARIO (2)

In the second scenario, we were applying the full algorithm described in Figure 1 to the same traffic situation. This means we were not only conditioning the tracks on fused or individual radar measurements, but also on AIS position data, if available. Figure 10 shows the resulting tracks for this multi-target scenario, in which two out of four mobile targets were also visible in AIS.

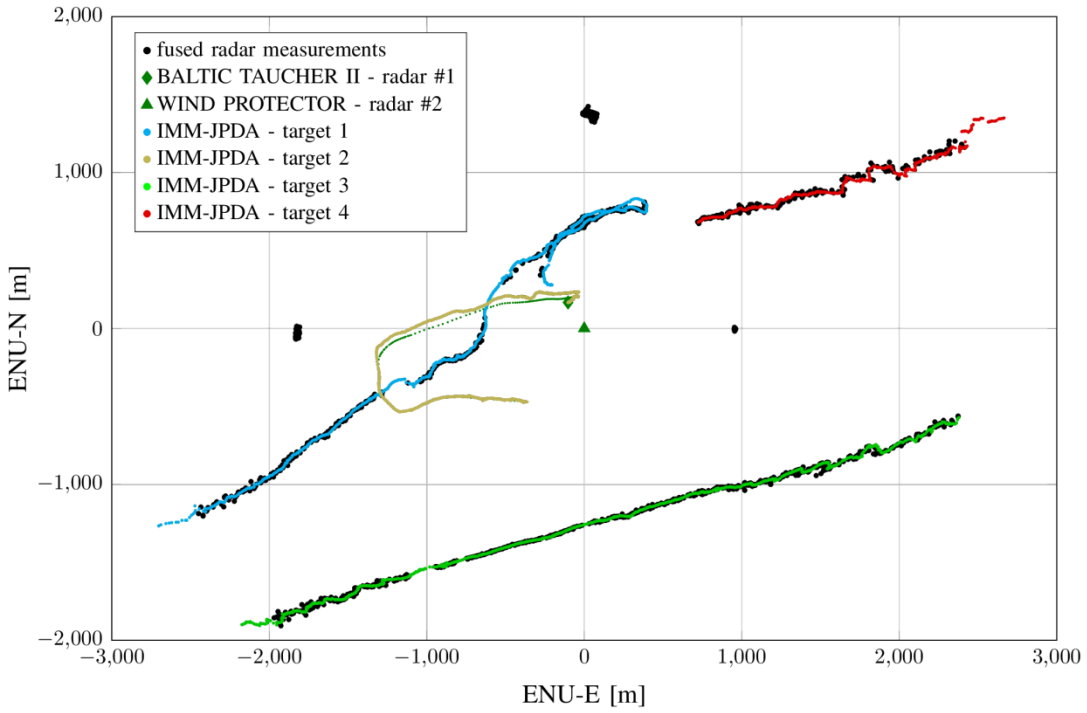

Figure 10: Results from multi-target tracking in a multi-radar setup fusing also AIS data.

Note, that one of these vessels (the BALTIC TAUCHER II) is also carrying one of the radars. The ship is included in the tracking process as it is visible in the other radar (at WIND PROTECTOR) as well as in the AIS. The black dotted clusters North-West and East from the stationary sensor platform are buoys. They were excluded from the tracking process since none of the dynamic process models was tuned to explain a stationary object. To tackle this in the future, a third model will be added to the IMM to keep track of these potential obstacles as well. As stated before, we cannot provide a quantified analysis concerning the multi-target tracking performance of our approach, clearly due to the lack of reference data. It has to be stated, though, that for situational awareness in the maritime domain the accurate positioning of surrounding vessels or objects down to the sub-meter level is of minor priority. We understand the completeness of the situation picture and the ability to separate objects from each other as higher ranked performance criteria. This also the primary motivation for fusing AIS with radar data in general; to gain a more robust and complete situation picture exploiting the complementary and diverse nature of different sensor sources.

3. CONCLUSION

In this work we have proposed an architecture to fuse data from a multi-radar sensor network prior to target tracking in an IMM-JPDA framework incorporating also AIS data. The main goal was to demonstrate the benefits of a cooperative scheme for traffic situation assessment which, in principle, is based on the idea of exchanging and fusing data between spatially distributed sensor nodes. In the maritime domain, each vessel or shore-based monitoring station can be understood as one of these nodes. We were proving the working principle of the proposed architecture on behalf of measurement data involving two radars installed on a mobile and on a stationary vessel monitoring the identical multi-target scenario. The reduction of uncertainty in the fused measurements could be shown to be a function of the aspect angle between both radars. It has to be noted, that the entire investigation was done in post-processing. This means, both radars were recorded simultaneously but independently, being synchronized via GPS time. We are aware of the fact, that the entire infrastructure that would enable real-time processing, including the physical layer or suitable network architecture, is an entire research field on its own.

In future, we will direct our research towards a more generic formulation of a distributed sensor network that allows for self-localization and multi-target tracking in a fully dynamic maritime scenario. To do so a number of open questions need to be addressed. First of all, for this work a perfect communication layer between both vessels was assumed. In a realistic setup additional effects such as latent or out-of-sequence data packages need to be considered as well. Secondly, the entire approach needs to be extended for fusing more than two radars. This affects not only the formalism for sensor fusion but also the network layer to provide efficient data handling among various nodes. Thirdly, for large scale traffic monitoring the currently applied JPDA filtering might be insufficient as its complexity scales combinatorially with more targets and more measurements.

REFERENCES

ITU Radiocommunication Sector (ITU-R) (2014), Technical characteristics for an automatic identification system using time division multiple access in the VHF maritime mobile band, Recommendation M.1371-5, ITU.

Bar-Shalom, Y., Daum, F. and Huang, J. (2009), The Probabilistic Data Association Filter, *IEEE CONTROL SYSTEMS MAGAZINE*.

Bhattacharyya, A. (1946), On a measure of divergence between two multinomial populations, *Sankhy: The Indian Journal of Statistics* (1933-1960) 7(4), pp. 401–406.

Blom, H. A. P. and Bar-Shalom, Y. (1988), The Interacting Multiple Model Algorithm for Systems with Markovian Switching Coefficients, *IEEE Transactions on Automatic Control,* 33.

Braca, P., Vespe, M., Maresca, S. and Horstmann, J. (2012), A Novel Approach to High Frequency Radar Ship Tracking Exploiting Aspect Diversity, *Geoscience and Remote Sensing Symposium (IGARSS)*, 2012 IEEE International, pp. 6895 – 6898.

Coraluppi, S., Carthel, C., Wu, C., Stevens, M., Douglas, J., Titi, G. and Luettgen, M. (2015), Distributed mht with active and passive sensors, In: *18th International Conference on Information Fusion (Fusion)*, pp. 2065–2072.

Drummond, O. E. and Blackman, S. S. (1989), Challenges of developing algorithms for multiple sensor, multiple target tracking.

Fortmann, T., Bar-Shalom, Y. and Scheffe, M. (1983), Sonar tracking of multiple targets using joint probabilistic data association, *IEEE Journal of Oceanic Engineering,* 8(3), pp. 173–184.

Glass, J. D., Blair, W. D. and Bar-Shalom, Y. (2013), IMM Estimators with Unbiased Mixing for Tracking Targets Performing Coordinated Turns, *Proceedings IEEE Aerospace Conference*.

Guerriero, M., Willett, P., Coraluppi, S. and Carthel, C. (2008), Radar/AIS Data Fusion and SAR tasking for Maritime Surveillance, In: *International Conference on Information Fusion,* Vol. 11.

Isard, M. and MacCormick, J. (2001), BraMBLe: A Bayesian multiple-blob tracker, In: *Eighth IEEE International Conference on Computer Vision*, Vol. 2, pp. 34–41.

Julier, S. J. and Uhlmann, J. K. (1997), A New Extension of the Kalman Filter to Nonlinear Systems, In: *Proceedings of AeroSense: The 11th Int. Symp. on Aerospace/Defence Sensing, Simulation and Controls.*, pp. 182–193.

Kalman, R. E. (1960), A new approach to linear filtering and prediction problem, *Trans. ASME* 82, 3445.

Kazimierski, W. and Stateczny, A. (2015), Radar and Automatic Identification System Track Fusion in an Electronic Chart Display and Information System, *THE JOURNAL OF NAVIGATION* (68), 1141–1154.

Khaleghi, B., Khamis, A., Karray, F. O. and Razavi, S. N. (2013), Multisensor data fusion: A review of the state-of-the-art, *Information Fusion* 14(1), 28 – 44.

Mahler, R. (2015), A brief survey of advances in random-set fusion, In: *Control, Automation and Information Sciences (ICCAIS), 2015 International Conference on*, pp. 62–67.

Mazzarella, F. and Vespe, M. (2015), SAR Ship Detection and Self-Reporting Data Fusion Based on Traffic Knowledge, *IEEE GEOSCIENCE AND REMOTE SENSING LETTERS*.

Munkres, J. (1957), Algorithms for the assignment and transportation problems, *Journal of the Society for Industrial and Applied Mathematics* 5(1), 32–38.

Perera, L. P., Ferrari, V., Santos, F. P., Hinostroza, M. A. and Soares, C. G. (2015), Experimental Evaluations on Ship Autonomous Navigation and Collision Avoidance by Intelligent Guidance, *IEEE JOURNAL OF OCEANIC ENGINEERING* 40.

Pulford, G. W. (2005), Taxonomy of multiple target tracking methods', IEEE Proceedings - Radar, *Sonar and Navigation* 152(5), 291–304.

Siegert, G., Banyś, P. and Heymann, F. (2016), Improving the Maritime Traffic Situation Assessment for a Single Target in a Multisensor Environment, In: *Proceedings of Maritime Knowledge Discovery and Anomaly Detection Workshop*, EC - JRC, Ispra, Italy, pp. 78–82.

Siegert, G., Banyś, P., Hoth, J. and Heymann, F. (2017), Counteracting the Effects of GNSS Jamming in a Maritime Multi-Target Scenario by Fusing AIS with Radar Data, In: *ION International Technical Meeting*, Institute of Navigation, Monterey, CA, USA.

Siegert, G., Banyś, P., Martínez, C. S. and Heymann, F. (2016), EKF Based Trajectory Tracking and Integrity Monitoring of AIS Data, In: *IEEE/ION Position, Location and Navigation Symposium - PLANS*, IEEE, Savannah, GA, pp. 887 – 897.

Tugnait, J. K. (2003), Tracking of multiple maneuvering targets in clutter using multiple sensors, imm and jpda coupled filtering, In: *Proceedings of the 2003 American Control Conference*, Vol. 2, pp. 1248–1253.